

Origin of the interhemispheric potential mismatch of merging cells for interplanetary magnetic field B_Y -dominated periods

Masakazu Watanabe,¹ George J. Sofko,¹ Konstantin Kabin,² Robert Rankin,² Aaron J. Ridley,³ C. Robert Clauer,^{3,4} and Tamas I. Gombosi³

Received 15 November 2006; revised 21 April 2007; accepted 25 May 2007; published 5 October 2007.

[1] When the dawn-to-dusk component of the interplanetary magnetic field (IMF B_Y) is dominant, ionospheric convection exhibits a basic two-cell pattern with significant dawn-dusk and interhemispheric asymmetries. For IMF $B_Y > 0$ the duskside merging cell potential in the Northern Hemisphere is much higher than that in the Southern Hemisphere, and the dawnside merging cell potential in the Southern Hemisphere is much higher than that in the Northern Hemisphere. The situation is reversed for IMF $B_Y < 0$. This interhemispheric potential mismatch originates from reconnection of overdraped lobe field lines and closed flankside field lines. This type of north-south asymmetric reconnection does not affect the merging cell potentials in the same hemisphere as the reconnection point, whereas in the opposite hemisphere, it diminishes the potential of the dawnside (or duskside) Dungey-type merging cell. Thus the total dawnside (or duskside) merging cell potential in one hemisphere is smaller than that in the other hemisphere by the reconnection voltage associated with the asymmetric reconnection.

Citation: Watanabe, M., G. J. Sofko, K. Kabin, R. Rankin, A. J. Ridley, C. R. Clauer, and T. I. Gombosi (2007), Origin of the interhemispheric potential mismatch of merging cells for interplanetary magnetic field B_Y -dominated periods, *J. Geophys. Res.*, *112*, A10205, doi:10.1029/2006JA012179.

1. Introduction

[2] It is well known that the global convection pattern in the ionosphere depends strongly on the orientation of the interplanetary magnetic field (IMF), which implies that the major driving mechanism of ionospheric convection is merging (or reconnection) of the IMF and the geomagnetic field. When the IMF B_Y component is dominant, ionospheric convection exhibits a distorted two-cell pattern with its dawn-dusk and interhemispheric asymmetries regulated by the IMF B_Y polarity. For IMF $B_Y > 0$ ($B_Y < 0$), in the northern ionosphere, the dawnside (duskside) cell is crescent-shaped, while the duskside (dawnside) cell is relatively round and extends to the dawnside (duskside) ionosphere beyond the noon meridian; the pattern in the southern ionosphere is basically a mirror image of the northern ionosphere with respect to the noon-midnight meridian [e.g., Burch *et al.*, 1985; Lu *et al.*, 1994]. In this paper, we use the terms “round cell” and “crescent cell” to describe the IMF B_Y -regulated convection cells. Burch *et al.* [1985] and Reiff and Burch [1985] interpreted the morphology

of ionospheric convection in terms of three kinds of convection cells: merging cells that intersect the open-closed field line boundary twice in one cycle, lobe cells that circulate exclusively in the open field line region of the ionosphere, and viscous cells that circulate exclusively in the closed field line region of the ionosphere. In this classic framework, the round cell consists of a merging cell and a lobe cell, while the crescent cell consists of a merging cell and a viscous cell.

[3] Crooker *et al.* [1998], in their magnetohydrodynamic (MHD) simulation study, addressed for the first time the interhemispheric potential mismatch of merging cells for IMF B_Y -dominated periods. They showed that the potential drop across a round merging cell in one hemisphere (the difference between the maximum and minimum potentials of the cell) was much higher than that across the crescent merging cell in the other hemisphere. Here, by “round merging cell,” we mean the merging-cell-proper part of the round cell (i.e., the lobe cell is excluded); similarly, by “crescent merging cell,” we mean the merging-cell-proper part of the crescent cell (i.e., the viscous cell is excluded). In order to reproduce this potential mismatch, using the latest BATS-R-US MHD code [Powell *et al.*, 1999], we performed a numerical simulation for the steady state magnetosphere-ionosphere system under pure IMF B_Y ($= 5$ nT) and typical solar wind ($V = 400$ km/s, $N = 5$ amu/cc, and $T = 50,000$ K) conditions. For simplicity we assumed uniform ionospheric conductances ($\Sigma_P = 3$ S and $\Sigma_H = 5$ S) and no dipole tilt. Figure 1 shows electric potentials in the northern ionosphere, with the dotted line indicating the open-closed field line boundary (which in this

¹Department of Physics and Engineering Physics, University of Saskatchewan, Saskatoon, Saskatchewan, Canada.

²Department of Physics, University of Alberta, Edmonton, Alberta, Canada.

³Department of Atmospheric, Oceanic, and Space Sciences, University of Michigan, Ann Arbor, Michigan, USA.

⁴Now at Department of Electrical and Computer Engineering, Virginia Polytechnic Institute and State University, Blacksburg, Virginia, USA.

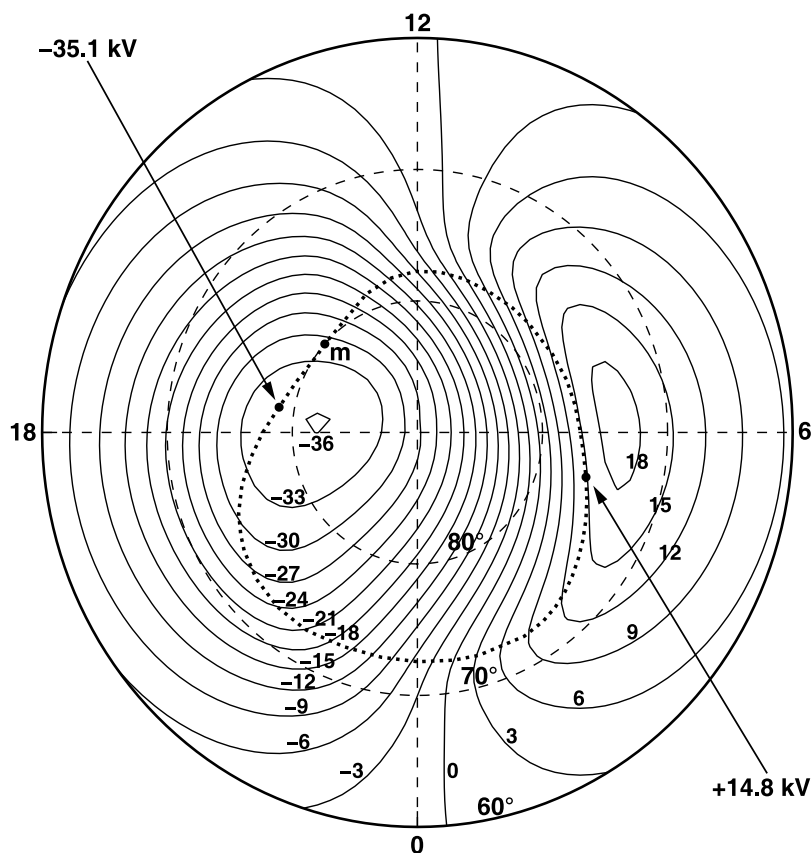


Figure 1. Simulated ionospheric potentials in the Northern Hemisphere (in kV) together with the open-closed field line boundary (the dotted line). The simulation parameters employed are as follows: interplanetary magnetic field (IMF) $B_X = 0$, $B_Y = 5$ nT, and $B_Z = 0$; solar wind velocity $V = 400$ km/s, density $N = 5$ amu/cc, and temperature $T = 50,000$ K; and uniform ionospheric conductances $\Sigma_H = 5$ S (Hall) and $\Sigma_P = 3$ S (Pedersen). There is no dipole tilt in this simulation. The arrows point to the locations of the potential maximum and minimum on the open-closed field line boundary. Point m indicates the footpoint of stemline s_1 from the magnetospheric null M as described in section 2.1.

paper we also call the “polar cap boundary”). As boundary conditions, the ionospheric potentials are set to zero at approximately 50 degrees of latitude, which is five degrees equatorward of the lowest latitude field-aligned current mapping. Potential patterns similar to Figure 1 were obtained by Crooker *et al.* [1998, Figure 3] and by Siscoe *et al.* [2001b, Figure 4]. The arrow on the dawnside (dusk-side) shows the potential maximum (minimum) on the polar cap boundary, and the potential values at the two points correspond to the potential drops across the merging cells. In this simulation, the crescent (round) merging cell potential is +14.8 kV (−35.1 kV). Since the potential pattern in the Southern Hemisphere consists of a crescent duskside cell at −14.8 kV and a round dawnside cell at +35.1 kV (the Hall conductance effect [Ridley *et al.*, 2004], which is the only source of breaking the mirror image pattern in this simulation, is negligible), there is a difference of 20.3 kV between the two hemispheres for both the dawnside and duskside merging cells. To our surprise, there has been little previous work that addressed this interhemispheric potential mismatch observationally. However, we can recognize the potential mismatch in the events studied by Lu *et al.* [1994, Figures 3 and 5 and Plates 1–4] (remember to compare only merging cell potentials). Thus, although observations are

very limited, we believe that the potential mismatch does exist in the actual magnetosphere-ionosphere system.

[4] Under the frozen-in magnetic flux condition, which holds true for the most part of the magnetosphere (except for the diffusion regions described below) and the F region ionosphere, plasma elements move along the equipotentials. Consequently, ionospheric convection cells manifest the magnetic flux circulation in the magnetosphere. In the steady state, the plasma elements cannot transfer from the dawnside convection cell to the duskside convection cell and vice versa, which means that the dawnside circulation and the duskside circulation are independent. Therefore, if the merging cell is driven exclusively by the merging of IMF lines and closed field lines on the dayside magnetopause and by the merging of north lobe and south lobe field lines in the magnetotail [Dungey, 1961], in the steady state, the potential drop across the dawnside (or duskside) merging cell should be the same in both hemispheres. Thus there must be another physical process that causes the interhemispheric potential difference. Crooker *et al.* [1998] suggested that the potential mismatch arose from the field-aligned potential drop along the field lines threading the diffusion region at the magnetopause. (The diffusion region is defined as a finite domain of “nonideal” plasma processes in which

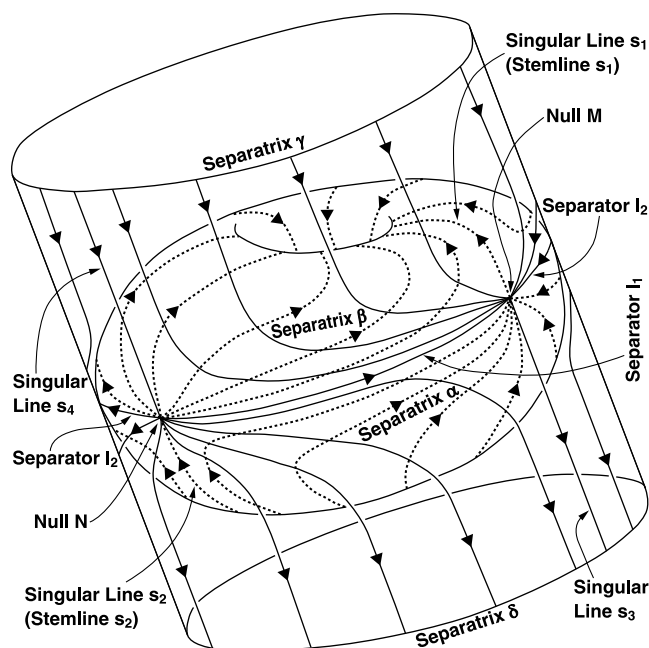


Figure 2. The separatrix surfaces (topologically a torus and a cylinder) resulting from superposition of a dipole field and a uniform IMF, with the arrowed lines representing magnetic field lines on the separatrix surfaces (not all kinds of field lines are shown). Field lines on the torus surface are shown by dotted lines, while field lines on the cylinder surface are shown by solid lines.

$\mathbf{E} + \mathbf{v} \times \mathbf{B}$ does not vanish [e.g., *Vasyliunas, 1975; Schindler et al., 1988*], where \mathbf{E} , \mathbf{v} , and \mathbf{B} represent, respectively, the electric field, plasma velocity, and magnetic field.) However, they did not show in detail where and how the potential drop occurred and how the field-aligned potential drop was related to the field-perpendicular potential drop in the ionosphere. Meanwhile, *Siscoe et al. [2001b]* calculated the field-aligned potential drop explicitly in their MHD model and found that a significant field-aligned potential drop existed not only along the dayside separator line where dayside reconnection was expected to occur but also along a field line on the separatrix (open-closed field line boundary) surface connecting the magnetic null in one hemisphere and the ionosphere in the other hemisphere (which they called the “dropline”). *Siscoe et al. [2001b]* concluded that the field-aligned potential drop along the dropline diminished the ionospheric potentials associated with the crescent cell. However, in their interpretation, they did not identify the physical process that causes the field-aligned potential drop.

[5] In MHD simulations, reconnection occurs from numerical magnetic diffusion. Therefore they cannot deal with the physical processes occurring inside the diffusion region. In this paper, using a conceptual merging model, we show that the field-aligned potential drop that causes the merging cell potential mismatch originates from the reconnection taking place between overdrafted lobe field lines and closed flankside field lines [*Tanaka, 1999; Watanabe et al., 2004, 2005, 2006*]. In order to understand the potential mismatch, it is necessary to understand the topology of field lines involved in reconnection. In sections 2–4, we describe step by step the complicated topology of the merging for IMF B_Y -dominated periods. Once the topology is obtained, the interhemispheric potential mismatch is understood as a corollary of the north-south asymmetric reconnection

(section 5). Finally, in section 6, we also refer to our MHD simulation results in Figure 1 and discuss their deviations from the conceptual merging model.

2. Topology Step 1: A Complete Set of Merging Types

[6] The first step is to introduce the null-separator topology and explore the possible types of merging in that topology. We show that there are sixteen types of merging in general.

2.1. Null-Separator Model

[7] The basic magnetic topology of the magnetosphere is expressed by superposing a dipole field and a uniform IMF in a vacuum [*Dungey, 1963; Cowley, 1973*]. This topology has a pair of magnetic null points and a pair of field lines joining the two nulls (see *Lau and Finn [1990, section 2]* for a review of general geometrical properties of such magnetic field configurations; also see *Fukao et al. [1975]* for a detailed discussion of the local magnetic field structure near null points). It has been shown that this vacuum-superposition topology also exists in MHD models [*Crooker et al., 1998; White et al., 1998; Siscoe et al., 2001a, 2001b; Watanabe et al., 2005*]. We call such magnetospheric models that are characterized by the vacuum-superposition topology the null-separator model.

[8] Figure 2, adapted from Figure 3 of *Watanabe et al. [2005]*, shows the separatrix surfaces of the null-separator model and is used to summarize the notation employed in this paper. The boundary between the open field line region and the closed field line region is topologically a torus, while the boundary between the open field line region and the IMF line region is topologically a cylinder. The internal (large) torus, which encompasses the (small) Earth, is

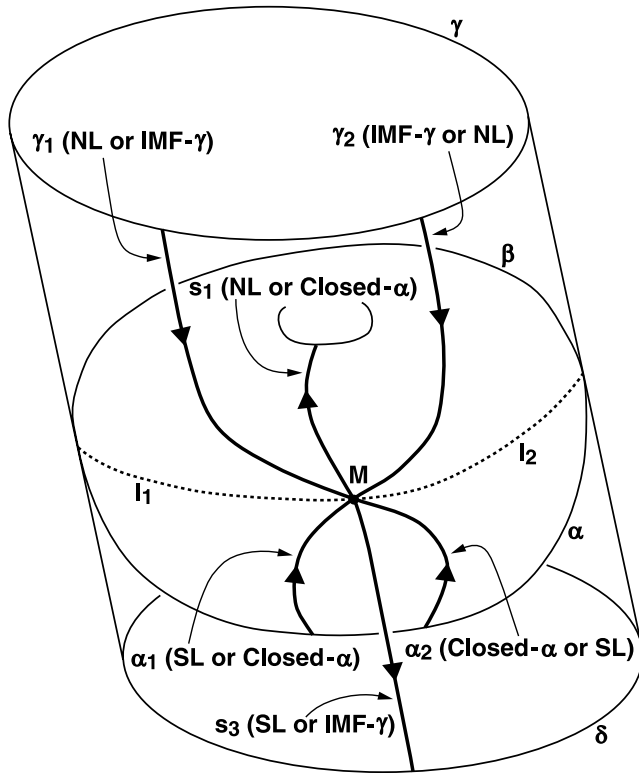


Figure 3. The elements of reconnecting field lines associated with null M. The annotation “SL or Closed- α ” or “Closed- α or SL” means that when α_1 represents a field line in South Lobe (or Closed- α), α_2 represents a field line in Closed- α (South Lobe). Similarly, the annotation “NL or IMF- γ ” or “IMF- γ or NL” means that when γ_1 represents a field line in North Lobe (or IMF- γ), γ_2 represents a field line in IMF- γ (North Lobe). Singular line s_1 (s_3) belongs to either North Lobe or Closed- α (either South Lobe or IMF- γ).

tangent to the cylinder along a circle. That circle consists of two magnetic field lines, called separators (l_1 and l_2 in Figure 2), connecting the two magnetic nulls (M and N in Figure 2) on the circle. We call the torus surface above (below) the separator circle separatrix β (separatrix α) and call the cylinder surface above (below) the separator circle separatrix γ (separatrix δ). All the field lines on separatrices α and γ converge to null M, except for the two singular field lines (s_2 on separatrix α and s_4 on separatrix γ) that converge to null N. Similarly, all the field lines on separatrices β and δ diverge from null N, except for the two singular lines (s_1 on separatrix β and s_3 on separatrix δ) that diverge from null M. Following *Siscoe et al.* [2001b], we call singular lines s_1 and s_2 “stemlines.” In the neighborhood of null M (null N), singular lines s_1 and s_3 (s_2 and s_4) are perpendicular to separatrices α and γ (β and δ).

[9] The entire space is divided into six topological regions by the four separatrices [*Watanabe et al.*, 2005, section 5]. The closed magnetic field line region consists of a subregion within separatrix α (Closed- α) and a subregion within separatrix β (Closed- β), the IMF line region consists of a subregion external to separatrix γ (IMF- γ) and a subregion external to separatrix δ (IMF- δ), and the open magnetic field line region consists of a subregion between separatrix β and separatrix γ (North Lobe) and a subregion

between separatrix α and separatrix δ (South Lobe). Note that well inside the torus, there is no definitive boundary between Closed- α and Closed- β . We distinguish the two only when we talk about the vicinity of the torus surface. Similarly, well outside the cylinder, there is no definitive boundary between IMF- γ and IMF- δ . In contrast, the distinction between North Lobe and South Lobe is straightforward; the North Lobe (South Lobe) field lines are connected to the northern (southern) ionosphere.

[10] The null-separator topology in Figure 2 is applicable to any orientations of the IMF and the Earth’s dipole axis, except when the IMF and the dipole axis are parallel. For example, at equinoxes with IMF $B_X = 0$, $B_Y > 0$ and $B_Z < 0$ ($B_X = 0$, $B_Y < 0$ and $B_Z < 0$) conditions, Figure 2 is a view from the Sun (magnetotail) with the top corresponding to the Northern Hemisphere. Another example is that at the boreal (austral) summer solstice with IMF $B_X < 0$, $B_Y = 0$, and $B_Z > 0$ ($B_X > 0$, $B_Y = 0$, and $B_Z > 0$) conditions, Figure 2 is a view from the duskside (dawnside) with the top (bottom) corresponding to the sunward direction.

2.2. Classification of Merging

[11] At null M, four topological regions (Closed- α , North Lobe, South Lobe, and IMF- γ) meet together. Similarly, at null N, four topological regions (Closed- β , North Lobe, South Lobe, and IMF- δ) meet together. For each null, merging occurs between the field lines of two such distinct regions. We enumerate and classify all the possible combinations of the two regions. Here we consider only the merging associated with null M. The discussion on the merging associated with null N is essentially the same. Figure 3 illustrates the elements of merging (reconnecting) field lines associated with null M. The merging field lines are interpreted to be on the surfaces of separatrices at the time of reconnection. All the field lines on separatrices α and γ (except for singular lines s_2 and s_4) converge to null M, and field lines on the same separatrix have the same topological characteristics. However, we should keep in mind that field lines on separatrix α belong to either South Lobe or Closed- α , while field lines on separatrix γ belong to either North Lobe or IMF- γ . Therefore, in counting merging field lines, we need to consider two distinct field lines (α_1 and α_2) on separatrix α and two distinct field lines (γ_1 and γ_2) on separatrix γ , as shown in Figure 3. The meaning of the annotation “SL or Closed- α ” or “Closed- α or SL” in Figure 3 is that when α_1 represents a field line in South Lobe (or Closed- α), α_2 represents a field line in Closed- α (South Lobe). Similarly, the meaning of “NL or IMF- γ ” or “IMF- γ or NL” is that when γ_1 represents a field line in North Lobe (or IMF- γ), γ_2 represents a field line in IMF- γ (North Lobe). Two of the four field lines (α_1 , α_2 , γ_1 , and γ_2) act as merging field lines that converge to null M. On the other hand, there are only two field lines (s_1 and s_3) diverging from null M, and both must always act as merging field lines. Considering the topological regions to which the converging field lines belong, we should interpret this topology as meaning that s_1 (s_3) belongs to either North Lobe or Closed- α (either South Lobe or IMF- γ). In summary, the merging field lines are two of the four converging field lines (α_1 , α_2 , γ_1 , and γ_2) and the two diverging field lines (s_1 and s_3).

[12] Since s_1 and s_3 must always participate in reconnection, possible cases of reconnection are determined by choosing two field lines from α_1 , α_2 , γ_1 , and γ_2 . Here we must choose two neighboring field lines for merging to occur. There are four possible combinations: merging of α_1 and γ_1 on separator l_1 , merging of γ_1 and γ_2 on separatrix γ , merging of α_1 and α_2 on separatrix α , and merging of α_2 and γ_2 on separator l_2 . (In this paper, when we say “separatrix α ,” for example, it does not include separators l_1 and l_2 on its edge. We distinguish reconnection on a separator and reconnection on a separatrix.) We first consider merging of α_1 and γ_1 on separator l_1 . There are two possible scenarios for this type of combination. The first scenario is that α_1 (or, more exactly, $\alpha_1 s_1$) representing a Closed- α field line merges with γ_1 ($\gamma_1 s_3$) representing an IMF- γ field line. In the second scenario, α_1 ($\alpha_1 s_3$) representing a South Lobe field line merges with γ_1 ($\gamma_1 s_1$) representing a North Lobe field line. Note that the combination of a Closed- α and a North Lobe field line (or a South Lobe and an IMF- γ field line) is topologically impossible because s_1 (s_3) cannot act simultaneously both as a Closed- α and a North Lobe field line (a South Lobe and an IMF- γ field line). Figure 4a shows merging of α_1 and γ_1 on separator l_1 . The field lines are not just on the separatrix surfaces but in their immediate neighborhood. The diffusion region occupies a three-dimensional volume around separator l_1 . In the case of merging of a Closed- α and an IMF- γ field line (a South Lobe and a North Lobe field line), the topology changes from the left panel to the right panel (from the right panel to the left panel). That is, one process is topologically the inverse of the other. Within the diffusion region, an electric field parallel to the magnetic field is allowed. This parallel electric field is proportional to the reconnection rate [Vasyliunas, 1984; Sonnerup, 1988] and is often called the reconnection (or merging) electric field. The direction of this electric field is the same as the direction of the electric current flowing in the diffusion region. It is also the same as the direction of the motional electric field ($-\mathbf{v} \times \mathbf{B}$, where \mathbf{v} is the plasma velocity and \mathbf{B} is the magnetic field) just outside the diffusion region. In the case of merging of a Closed- α and an IMF- γ field line (a South Lobe and a North Lobe field line), the merging electric field is directed toward (away from) null M along separator l_1 . From the above consideration we learn that once the merging location (separator l_1 in this case) and the direction of the merging electric field (toward null M, for example) are given, the merging field lines (a Closed- α and an IMF- γ field line) and the resultant field lines (a South Lobe and a North Lobe field line) are uniquely specified. It is easily verified that this is true for the other three merging locations as shown in Figure 4b (merging on separatrix γ), Figure 4c (merging on separatrix α), and Figure 4d (merging on separator l_2).

[13] Thus the possible cases of reconnection are enumerated by specifying the merging location and the direction of the reconnection electric field in the diffusion region. As noted above, there are four possible merging locations: separator l_1 (Figure 4a), separatrix γ (Figure 4b), separatrix α (Figure 4c), and separator l_2 (Figure 4d). For each merging location, two types of merging are possible depending on whether the reconnection electric field is toward or away from null M, with one type being the

inverse process of the other. In Figure 4, reconnection with an electric field toward (away from) null M proceeds from the left panel to the right panel (from the right panel to the left panel). Thus there are eight distinctive types of merging associated with null M. These types are summarized in Table 1 (the top eight rows). Exactly the same reasoning is applied to the merging cases associated with null N (the bottom eight rows in Table 1). We here denote a merging type in which the electric field is toward (away from) the null by the plus (minus) sign. The Latin letters representing the types (A to H) are chosen to be as consistent as possible with *Watanabe et al.* [2005]. In total, there are 16 types of merging in the null-separator model.

[14] We can apply the classification of Table 1 to any orientations of the IMF and the dipole axis, except when the IMF and the dipole axis are parallel. For example, the duskside type A to type D reconnection discussed by *Watanabe et al.* [2005, 2006] correspond to type A+, type B+, type C+, and type D+ in Table 1, respectively. Note that *Watanabe et al.* [2005, 2006] did not need to distinguish dawnside and duskside reconnection and used the same notation (type A to type D) for both dawnside and duskside. The dawnside type A to type D reconnection of *Watanabe et al.* [2005, 2006] correspond to type G–, type H–, type C–, and type D– in Table 1, respectively.

3. Topology Step 2: Merging Types for IMF B_Y -Dominated Periods

[15] The next step is to examine, considering a concrete geometry of the field lines, which types of merging are physically possible for IMF B_Y -dominated periods. We show that eight out of the sixteen merging types can reasonably occur.

3.1. Null-Separator Topology in the Simulated Magnetosphere

[16] We first need to know the specific geometry of the null-separator structure. Figure 5 shows a three-dimensional view of the torus determined in our MHD simulation for pure IMF B_Y ($= 5$ nT), with blue and red lines respectively representing separatrices α and β ; more precisely, Figure 5 shows the last closed field lines earthward of separatrices α and β . The X , Y , and Z axes are those in Geocentric Solar-Magnetospheric (GSM) coordinates. Similar results were obtained by *Siscoe et al.* [2001b, Figure 2]. The intersection of separatrix α (separatrix β) and the southern (northern) ionosphere forms a closed curve called the polar cap boundary. The blue (red) lines in Figure 5 start from the southern (northern) polar cap boundary and converge to almost a single point in the Northern (Southern) Hemisphere. This converging point corresponds to null M (null N) in Figure 2. Subsequently, the converged field lines go to the northern (southern) ionosphere as a tight bundle of field lines. This bundle of lines corresponds to stemline s_1 (stemline s_2) in Figure 2. The footpoint of stemline s_1 is shown in Figure 1 by point m. The locations of the two nulls determined by searching magnetic field minima are $(X, Y, Z) = (-1.25, \pm 10.25, \pm 10.5) R_E$ with an accuracy of $0.25 R_E$ (the cell size in the vicinity of the nulls). On the dayside, we can recognize the presence of a field line connecting the two nulls along the tangential line between the blue and the red

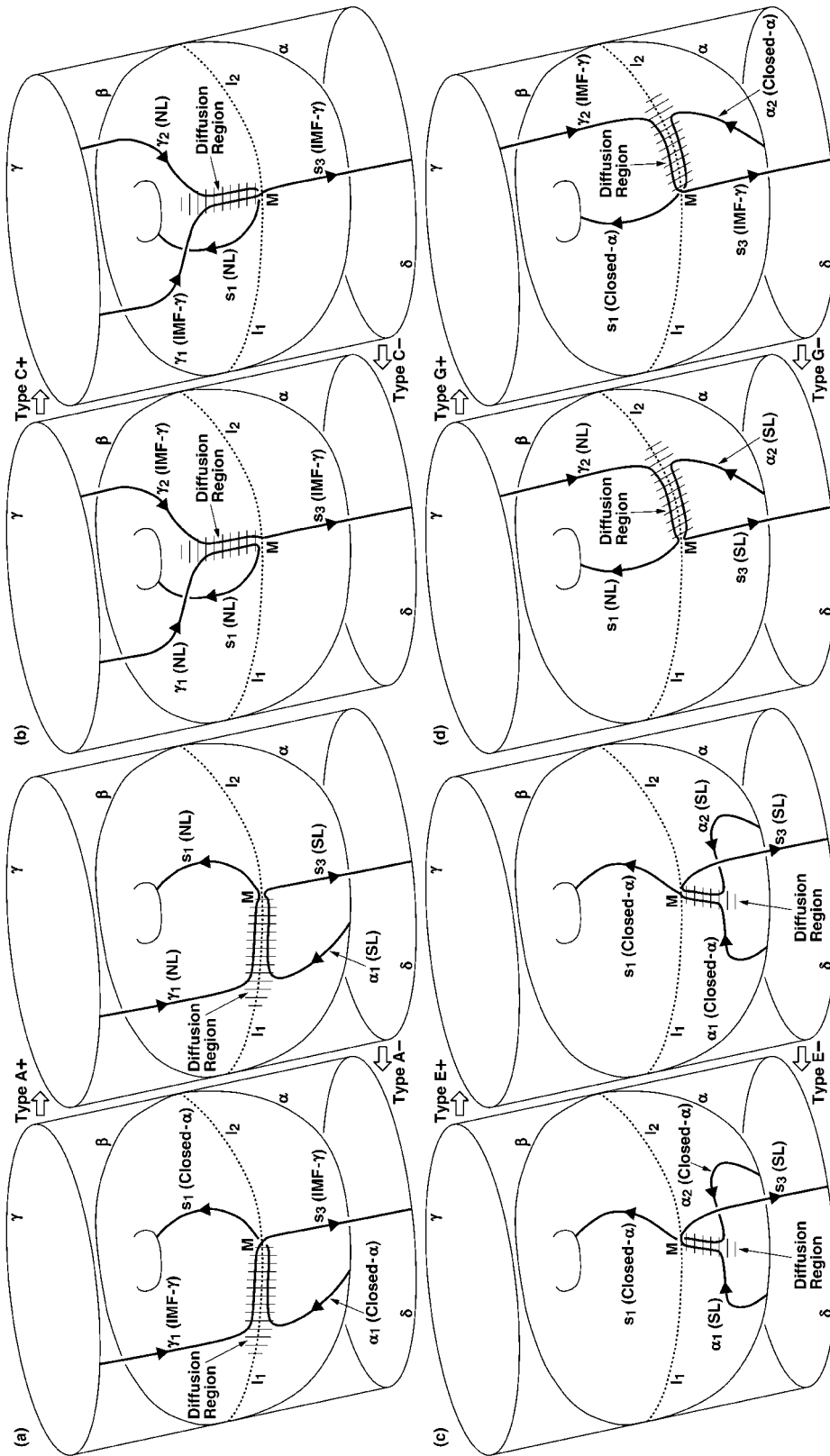


Figure 4. (a–d) Magnetic field topology of the eight possible cases of reconnection associated with null M. The field lines are not just on the separatrix surfaces but in their immediate neighborhood. The hatched pattern schematically represents the diffusion regions where field lines merge. Each diffusion region occupies a three-dimensional volume around the separator line (Figures 4a and 4d) or the similar “center-of-merging” line on the separatrix surface (Figures 4b and 4c). For plus-type (minus-type) reconnection, the topology changes from the left (right) panel to the right (left) panel.

Table 1. Merging in the Null-Separator Model

| Type | Null | Diffusion Region | Electric Field | Merging Field Lines | Resultant Field Lines |
|------|------|---------------------|----------------|----------------------------------|----------------------------------|
| A+ | M | separator l_1 | toward | Closed- α , IMF- γ | North Lobe, South Lobe |
| A- | M | separator l_1 | away | North Lobe, South Lobe | Closed- α , IMF- γ |
| C+ | M | separatrix γ | toward | IMF- γ , North Lobe | IMF- γ , North Lobe |
| C- | M | separatrix γ | away | IMF- γ , North Lobe | IMF- γ , North Lobe |
| E+ | M | separatrix α | toward | Closed- α , South Lobe | Closed- α , South Lobe |
| E- | M | separatrix α | away | Closed- α , South Lobe | Closed- α , South Lobe |
| G+ | M | separator l_2 | toward | North Lobe, South Lobe | Closed- α , IMF- γ |
| G- | M | separator l_2 | away | Closed- α , IMF- γ | North Lobe, South Lobe |
| B+ | N | separator l_1 | toward | North Lobe, South Lobe | Closed- β , IMF- δ |
| B- | N | separator l_1 | away | Closed- β , IMF- δ | North Lobe, South Lobe |
| D+ | N | separatrix β | toward | Closed- β , North Lobe | Closed- β , North Lobe |
| D- | N | separatrix β | away | Closed- β , North Lobe | Closed- β , North Lobe |
| F+ | N | separatrix δ | toward | IMF- δ , South Lobe | IMF- δ , South Lobe |
| F- | N | separatrix δ | away | IMF- δ , South Lobe | IMF- δ , South Lobe |
| H+ | N | separator l_2 | toward | Closed- β , IMF- δ | North Lobe, South Lobe |
| H- | N | separator l_2 | away | North Lobe, South Lobe | Closed- β , IMF- δ |

line surface. (In Figure 5, in the neighborhood of the tangential line, a blue and a red line are overlapped with the red line behind the blue line.) This field line corresponds to separator l_1 in Figure 2. We can also recognize envelope curves directed tailward away from the two nulls. These envelopes represent part of separator l_2 in Figure 2. However, the magnetotail portion of separator l_2 is not visible in Figure 5; the detailed configuration of separator l_2 will become clear in Figure 6, which we discuss next.

[17] Figure 6 shows a front view (Figure 6a) and a top view (Figure 6b) of separatrix γ ; more precisely, Figure 6 shows the last open (Earth-connected) field lines earthward of separatrix γ . Similar results were obtained by Crooker *et al.* [1998, Figure 1]. For clarity, we do not show separatrix δ in Figure 6. Separatrix δ is obtained by rotating separatrix γ 180° about the X axis. All field lines on the dawnside open-interplanetary field line boundary converge to null M and go to the northern ionosphere virtually as one field line (stemline s_1). In Figure 6 we can clearly identify an

envelope curve connecting the two nulls. This is separator l_2 of the nightside magnetosphere. The so-called “magnetospheric sash” [White *et al.*, 1998] is a ribbon of weak magnetic field that runs along a magnetopause section of separator l_2 . In Figure 6a, separator l_2 has a sigmoid shape; White *et al.* [1998] called this characteristic shape “cross-tail S.” As delineated by separator l_2 in Figure 6b, the shape of the torus has “wings” on the flanks [Song *et al.*, 2001]. In summary, Figures 5 and 6 clearly indicate the presence of the null-separator topology in the MHD simulated magnetosphere.

3.2. Antiparallel Field Line Configurations

[18] We now consider possible reconnection topologies for periods of IMF $B_Y > 0$ and no dipole tilt. Since the system is symmetric with respect to the GSM X axis, it is sufficient to consider merging associated with null M. Generally, reconnection (i.e., diffusion) occurs where there is some antiparallel component of neighboring magnetic

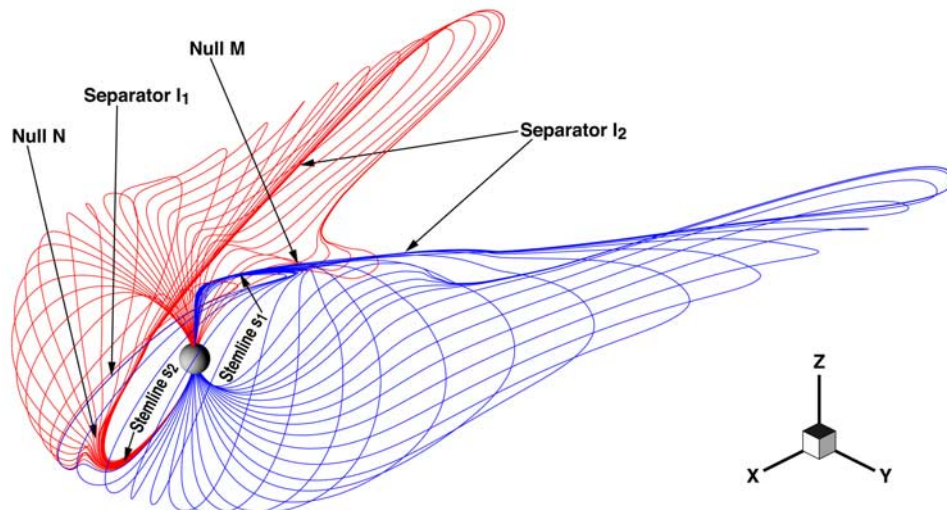


Figure 5. A three-dimensional view of the torus in the MHD simulation. Blue lines represent separatrix α , while red lines represent separatrix β .

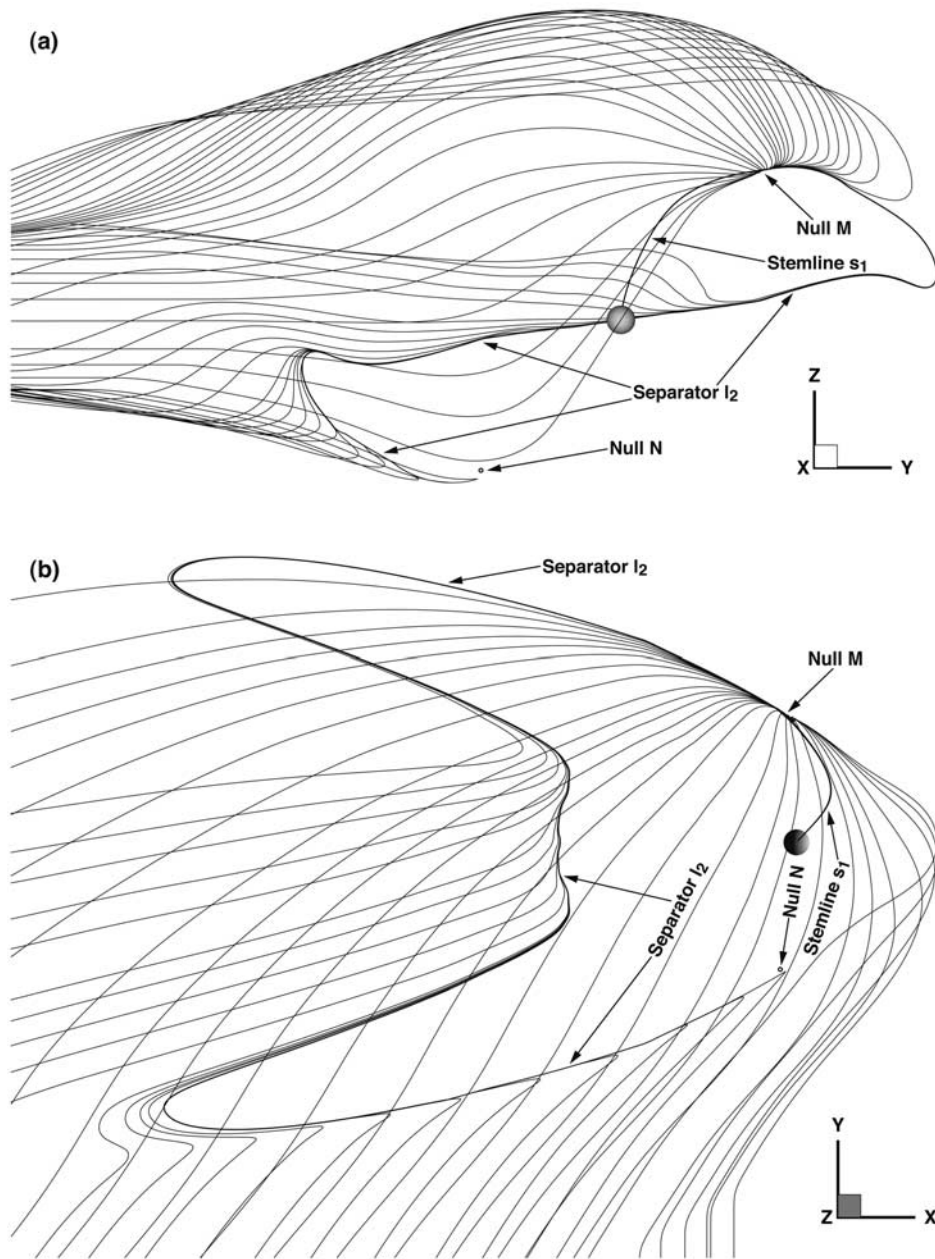


Figure 6. Projection views of separatrix γ in the MHD simulation (a) in the Y - Z plane and (b) in the X - Y plane.

fields. For each type of reconnection in Figure 4, we examine whether the reconnecting field lines form an antiparallel configuration under the separatrix geometry in Figures 5 and 6. We realize that for each of Figures 4a–4d, either the plus type or the minus type can produce a reasonable antiparallel configuration. The left panels of Figure 7 depict such schematic antiparallel configurations, with Figures 7a–7d corresponding to Figures 4a–4d, respectively. All figures are views from the Sun, and merging occurs around the cross in each figure. The resultant reconnected field lines are shown in the right panels. Note that field line geometry is somewhat deformed so that the antiparallel nature of the reconnecting field lines becomes evident. The dots on the field lines in Figure 7

indicate plasma elements attached to the reconnecting and the reconnected field lines. For each type of reconnection, we associate one pair of plasma elements with each of the two reconnecting lines (for example, A_1 to A_4 for type A^+). We interpret the transition of the topological region to which each plasma element belongs as a plasma flow across the separatrix associated with reconnection [cf. *Watanabe et al.*, 2005, section 5]. Subscripts 1–4 are defined consistently with Figure 1 of *Watanabe et al.* [2005]. Subscript 4 is assigned to the plasma element on the stemline, and subscript 2 is assigned to the plasma element on the other singular line. For plus-type merging, plasma elements with subscripts 1 and 2 are on one of the reconnecting field lines before reconnection, while plasma elements 3 and 4 are on

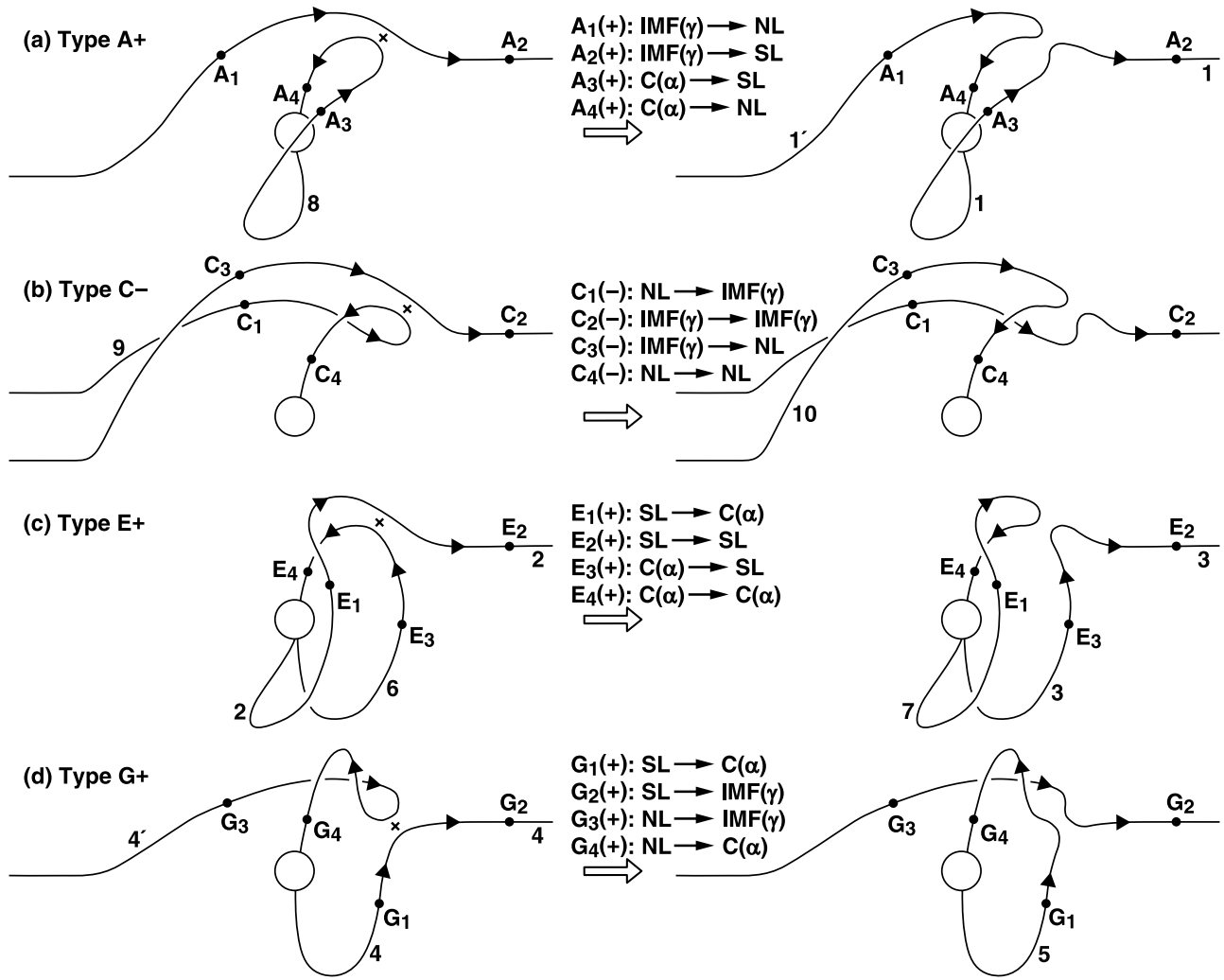


Figure 7. (a–d) Schematics representing the field line geometry of the four types of duskside (null M-associated) reconnection for IMF $B_Y \gg |B_Z|$ viewed from the Sun. The crosses show the centers of the diffusion regions. For each type of reconnection, four kinds of topological region transitions are identified: A₁(+) to A₄(+) for type A+, C₁(–) to C₄(–) for type C–, E₁(+) to E₄(+) for type E+, and G₁(+) to G₄(+) for type G+. Abbreviations of topological regions are as follows: IMF, Interplanetary Magnetic Field; C, Closed; NL, North Lobe; and SL, South Lobe.

the other reconnecting line. Therefore, for example, A₁ to A₄ in Figure 7a directly correspond to A₁ to A₄ in Figure 1a of Watanabe et al. [2005].

[19] Let us summarize the four types of reconnection in Figure 7 in terms of the null-separator model (see Table 1). Type A+ reconnection (Figure 7a) is merging of IMF- γ and Closed- α field lines on separator l_1 with the reconnection electric field directed toward null M; type C– reconnection (Figure 7b) is merging of IMF- γ and North Lobe field lines on separatrix γ with the reconnection electric field directed away from null M; type E+ reconnection (Figure 7c) is merging of Closed- α and South Lobe field lines on separatrix α with the reconnection electric field directed toward null M; type G+ reconnection (Figure 7d) is merging of North Lobe and South Lobe field lines on separator l_2 with the reconnection electric field directed toward null M.

[20] In the description below, we consider only duskside reconnection for $B_Y > 0$. Dawnside and duskside reconnection are symmetric with respect to the X axis. For $B_Y > 0$,

the types of dawnside reconnection that correspond to the reconnection geometries in Figures 7a–7d are type B–, type F+, type D–, and type H–, respectively. For $B_Y < 0$, null M and null N switch in position and so do separators l_1 and l_2 . Namely, null M (null N) is on the dawnside (duskside), and separator l_1 (separator l_2) is on the nightside (dayside). In this case, the types of dawnside (duskside) reconnection that correspond to the reconnection geometries in Figures 7a–7d are type G–, type C+, type E–, and type A– (type H+, type F–, type D+, and type B+), respectively.

4. Topology Step 3: Effects of the Normal Magnetic Field Component

[21] The final step is to modify the null-separator topology for the purpose of qualitative understanding of the magnetosphere-ionosphere coupling by adding a small normal component of the magnetic field to the separatrix surface.

This is equivalent to considering a zero-thickness diffusion region.

4.1. Current Penetration Model

[22] In the null-separator model, the electric potentials at the earthward edge of the diffusion regions are mapped to the ionosphere along the assumed equipotential field lines. Thus we must know the electric fields inside the diffusion regions in order to know the potentials in the ionosphere. However, it is practically very difficult to determine the extent of the diffusion regions and to assess the parallel electric fields. Therefore the orthodox approach based on the null-separator model does not provide a good insight into the problem. In order to surmount this difficulty, we employ the method of the current penetration model as *Watanabe et al.* [2005, section 6] did. The merit of the current penetration model is that it circumvents the detailed description of the diffusion regions and provides the results equivalent to the null-separator model for global phenomena occurring far away from the diffusion regions.

[23] The current penetration model is a generic name of merging models that involve a normal component of the magnetic field (B_N) on the boundary between the two regions of merging field lines. This class of merging models was first proposed by *Alekseyev and Belen'kaya* [1983] and later developed by *Crooker et al.* [1990]. In general, the topology of a current penetration model is obtained by adding small B_N to a separatrix surface of the vacuum null-separator topology. The perturbation field B_N is controlled by the electric currents confined to an infinitesimally thin layer on the boundary (i.e., the former separatrix that has become a rotational discontinuity). The diffusion effects are attributed entirely to these boundary currents. Since the magnetic field penetrates this current layer, *Siscoe* [1988] called this kind of merging model the current penetration model. The current penetration model is highly flexible so that one can add almost any penetration magnetic field, globally or locally, by choosing an appropriate boundary current.

[24] On the one hand, adding B_N globally to a separatrix destroys the null-separator topology. On the other hand, the null-separator topology is stable to magnetic field perturbations and cannot be destroyed easily [*Greene*, 1988]. These paradoxical features are reconciled if one recognizes that the “global” current penetration model with an infinitesimally thin current layer is topologically equivalent to the null-separator model with a finite thickness diffusion region [*Siscoe*, 1988; *Crooker*, 1990; *Crooker et al.*, 1990, 1998]. If the diffusion region in the null-separator model collapses into a surface, the null is confined to the boundary and effectively disappears. Conversely, when the boundary current in the current penetration model occupies a finite thickness, the null reappears within the current layer. In other words, in global current penetration models, the null-separator topology is found within the thin current layer. Thus we can say that the null-separator model and the (global) current penetration model are basically the same merging model. The difference is the spatial scale on which one observes the diffusion region. It should be noted here, however, that the “local” current penetration model is not always consistent with the null-separator topology. If the penetration field is confined to a patchy region on a

separatrix, reconnection can occur without nulls as modeled for flux transfer events by *Hesse et al.* [1990]. Otherwise, however, nulls are very stable aspects of magnetic topology [*Greene*, 1988], and one cannot dissociate nulls from merging. The current penetration model and its relation to the null-separator model are extensively reviewed by *Siscoe* [1988] and *Crooker* [1990].

4.2. Transformation From Null-Separator to Current Penetration Model

[25] From the null-separator model in Figure 4, we now develop the topology of the current penetration model for the four types of reconnection in Figure 7. As noted in section 4.1, the current penetration model is interpreted to be the limit of the null-separator model when the thickness of the diffusion region goes to zero. Hence we must find an appropriate distribution of B_N that is consistent with Figure 4. In the current penetration model, an X (merging) line is formed where the sign of B_N reverses. On both sides of the X line, because of B_N , the reconnecting field lines from the two neighboring regions are linked directly without an excursion to the remote null. Considering these characteristics, we first locate the X line along the center of the diffusion region in the null-separator model in Figure 4 (for example, separator l_1 for type A+). On the separatrix(ices) adjacent to the X line (both the torus and cylinder for type A+), we next add a small perturbation field B_N that changes its sign across the X line. The sign of B_N should be chosen so that on each side of the X line, B_N connects the merging field lines from the two regions (IMF- γ and Closed- α for type A+). Figure 8 shows magnetic field topology of the current penetration model thus obtained for the four types of reconnection, with Figures 8a–8d corresponding to Figures 4a–4d, respectively. The open arrows represent the reconnection electric field on the X line. Symbols A_1 to A_4 , C_1 to C_4 , E_1 to E_4 , and G_1 to G_4 , which were originally introduced to designate plasma elements attached to the reconnecting or reconnected field lines (Figure 7), are now used instead to designate bundles of field lines that emanate from the infinitesimally near neighborhood of the X line. The X line (which is a so-called “guide field” line) is anchored to the magnetic null at one end, where the reconnecting field lines become strictly antiparallel.

[26] We add some notes for each type of reconnection:

[27] 1. For type A+ (Figure 8a), inward (outward) B_N has been added on separatrices β and γ (separatrices α and δ) in the neighborhood of the X line. A_1 and A_2 run outside the cylinder keeping an infinitesimally small distance from the cylinder surface. A_3 and A_4 run inside the torus keeping an infinitesimally small distance from the torus surface.

[28] 2. For type C– (Figure 8b), inward (outward) B_N has been added on separatrix γ in the l_1 -side (l_2 -side) neighborhood of the X line. C_1 (C_3) runs inside (outside) the cylinder keeping an infinitesimally small distance from the cylinder surface. C_2 (C_4) is located outside the cylinder (torus) at a finite distance away from the cylinder (torus) surface.

[29] 3. For type E+ (Figure 8c), inward (outward) B_N has been added on separatrix α in the l_1 -side (l_2 -side) neighborhood of the X line. E_1 (E_3) runs outside (inside) the torus keeping an infinitesimally small distance from the torus surface. E_2 (E_4) is located inside the cylinder (torus) at a finite distance away from the cylinder (torus) surface.

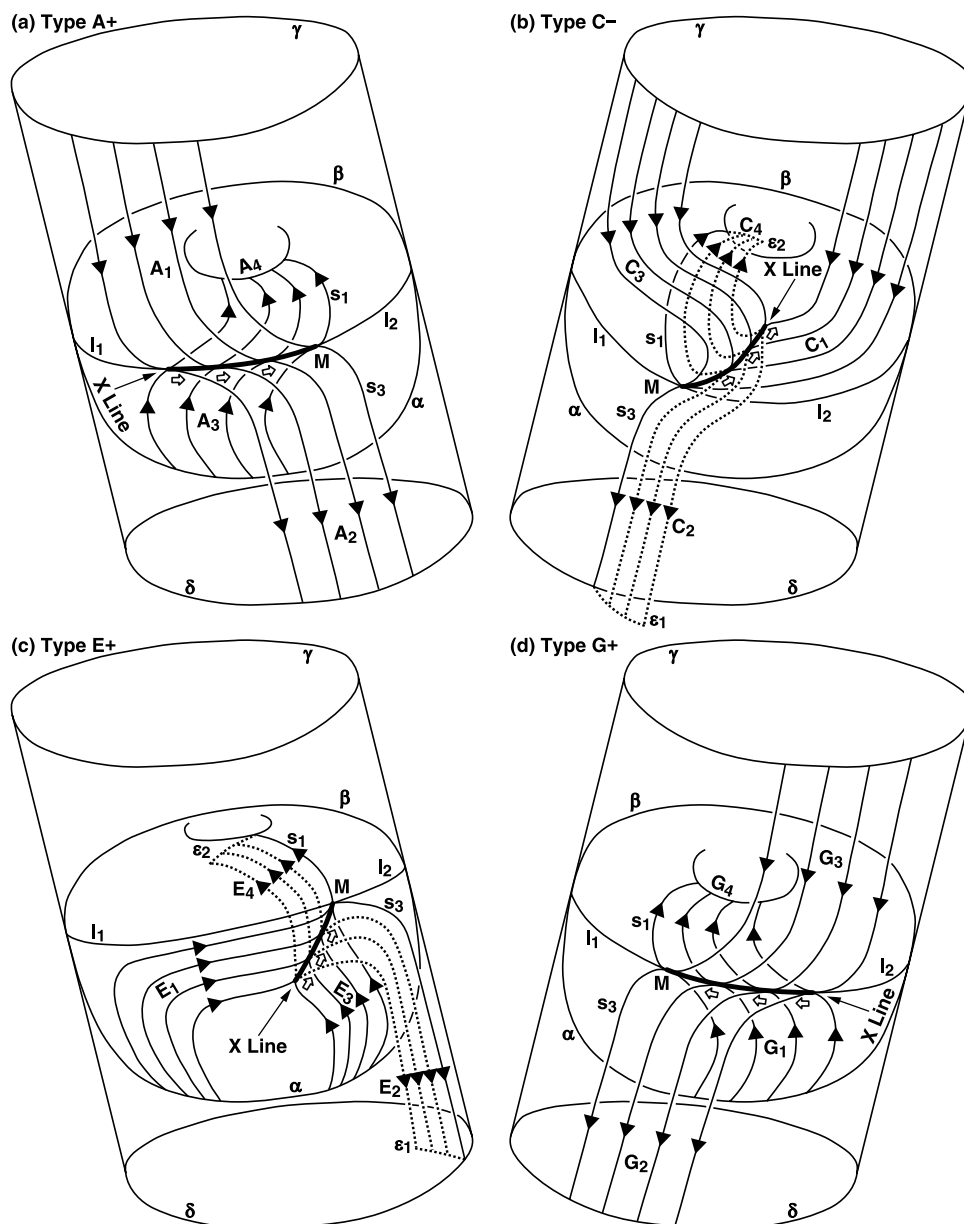


Figure 8. (a–d) The current penetration models of the four types of reconnection in Figure 7. Symbols A_1 to A_4 , C_1 to C_4 , E_1 to E_4 , and G_1 to G_4 correspond to those in Figure 7, respectively, but are used here to designate field lines emanating from the infinitesimally near neighborhood of the X line. Solid field lines are on the torus and cylinder surfaces, while dotted field lines (C_2 , C_4 , E_2 , and E_4) are away from the torus and cylinder surfaces. The open arrows indicate the direction of the electric field on the X line. In Figure 8b (Figure 8c), ε_1 and ε_2 represent the surfaces formed by field lines C_2 and C_4 (E_2 and E_4), respectively.

[30] 4. For type G+ (Figure 8d), outward (inward) B_N has been added on separatrices β and γ (separatrices α and δ) in the neighborhood of the X line. G_2 and G_3 run inside the cylinder keeping an infinitesimally small distance from the cylinder surface. G_1 and G_4 run outside the torus keeping an infinitesimally small distance from the torus surface.

[31] The finite displacement of C_2 and E_2 (C_4 and E_4) from the cylinder (torus) surface requires an explanation. Here we explain for the C_2 and C_4 cases (Figure 8b). In the unperturbed state, field line C_2 (C_4) emanating from the X line on separatrix γ first goes to null M along the X line and

then goes to infinity (to the northern ionosphere) along s_3 (s_1). When a perturbation field B_N is added to separatrix γ , the field line path deviates from the above unperturbed path. The perturbed path is on a curved surface that contains the X line and s_3 (s_1). Let this surface be called ε_1 (ε_2). The surface ε_1 (ε_2) intersects separatrix δ (separatrix β) along s_3 (s_1) at nonzero angles. (While ε_1 (ε_2) is defined by s_3 (s_1) and the X line, separatrix δ (separatrix β) is defined by s_3 (s_1) and separator l_1 or l_2). In the neighborhood of null M, s_3 (s_1) is perpendicular to separatrix γ on which both the X line and the separator are located, and the X line

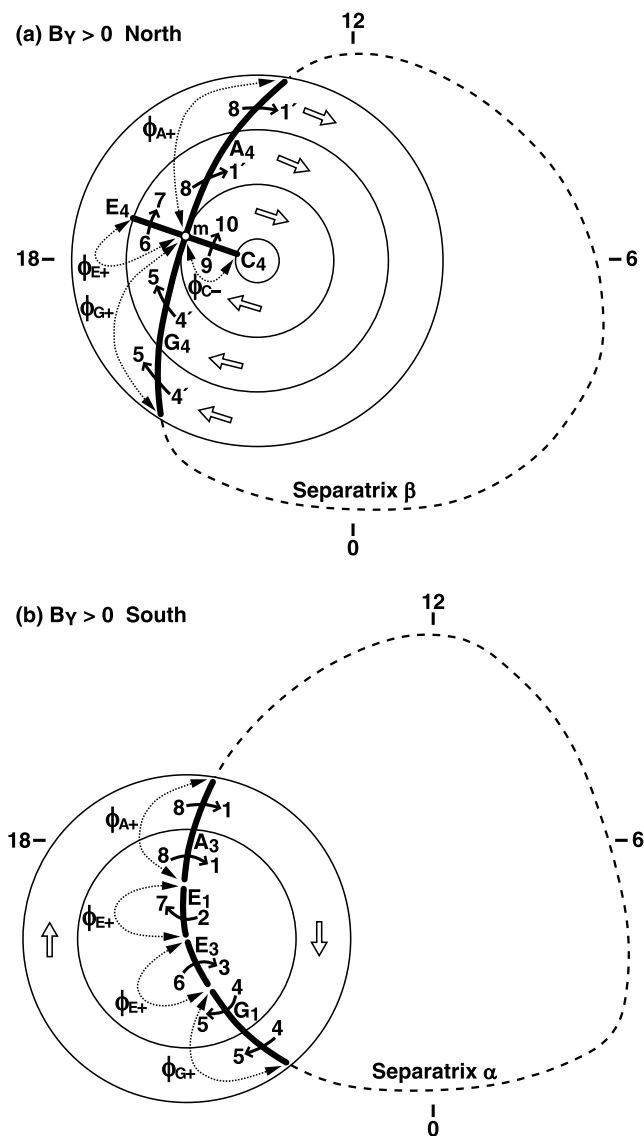


Figure 9. The consequences of the four types of reconnection in Figure 7 (a) in the northern ionosphere and (b) in the southern ionosphere. The open arrows indicate the direction of ionospheric convection. The D-shaped loops show the open-closed field line boundaries (i.e., separatrices α and β). The thick lines with symbols A_3 , A_4 , C_4 , E_1 , E_3 , E_4 , G_1 , and G_4 indicate the ionospheric projection of the X lines along the corresponding field lines in Figure 8. The numbers 1–10, 1', and 4' are the footpoints of the corresponding field lines in Figure 7. The solid arrows connecting these numbers show magnetic flux transport across the projected X lines. The dotted two-headed arrows are labeled with the potential difference between the two endpoints of the projected X line.

and the separator intersect at nonzero angles at null M.) In the vicinity of null M, the direction of the magnetic field changes significantly on a very short spatial scale. Consequently, after passing null M, C_2 (C_4) on ε_1 (ε_2) deviates from s_3 (s_1) by a finite amount even if B_N is very small. Therefore C_2 (C_4) is located at a finite distance away from

separatrix δ (separatrix β). The situation is exactly the same for the E_2 and E_4 cases (Figure 8c). If, in the above description, C_2 , C_4 , and separatrix γ are replaced by E_2 , E_4 , and separatrix α , respectively, the explanation for E_2 and E_4 is obtained. In Figure 8, field lines C_2 , C_4 , E_2 , and E_4 that are away from the separatrix surface are represented by dotted lines. In contrast, the other field lines (A_1 , A_2 , A_3 , A_4 , C_1 , C_3 , E_1 , E_3 , G_1 , G_2 , G_3 , and G_4) that are virtually on the separatrix surface are represented by solid lines in Figure 8.

5. Consequences of the Merging for IMF B_Y -Dominated Periods

5.1. Ionospheric Convection

[32] Each type of reconnection in Figure 7 has a unique signature in ionospheric convection. Using the reconnection electric fields in Figure 8, we map the reconnection electric fields to the ionosphere. Figure 9 shows the expected duskside convection pattern in the ionosphere driven by the four types of reconnection, with the open arrows indicating the direction of the convection. The D-shaped loops indicate separatrices α and β (i.e., the polar cap boundaries). Point m in Figure 9a is the footpoint of stemline s_1 connecting null M and the northern ionosphere; this point should be called the topological “cusp” (see Figure 3 of Crooker [1992] and Figure 2 of Watanabe et al. [2006]). The thick solid lines show the ionospheric projection of the X lines (A_3 , A_4 , C_4 , E_1 , E_3 , E_4 , G_1 , and G_4 in Figure 8). In the Northern Hemisphere, all the projected X lines converge to the cusp. The solid arrows indicate the direction of the magnetic flux transport across the projected X lines, with numbers 1–10, 1', and 4' representing the footpoints of the field lines in Figure 7 labeled with the same number. The dotted two-headed arrows are labeled with the potential difference between the two endpoints of the projected X line. The potential difference is equal to the reconnection voltage ϕ (with the subscript indicating the type of reconnection) that is positive and is defined as the electric field integrated along the X line.

[33] The X line of type A+ reconnection is mapped to a segment of the polar cap boundary for both hemispheres (A_4 in Figure 9a and A_3 in Figure 9b). Therefore type A+ reconnection drives a closed-to-open flow across the dayside polar cap boundary for both hemispheres. Similarly, the X line of type G+ reconnection is mapped to a segment of the polar cap boundary for both hemispheres (G_4 in Figure 9a and G_1 in Figure 9b). Therefore type G+ reconnection drives an open-to-closed flow across the nightside polar cap boundary for both hemispheres. Thus type A+ and type G+ reconnection form a merging cell on the duskside for both hemispheres, which may be called the Dungey-type merging cell [Dungey, 1961].

[34] The X line of type C– reconnection is mapped to a line inside the northern polar cap (C_4 in Figure 9a) owing to the B_N effect on the ε_2 surface (Figure 8b). Therefore type C– reconnection drives a sunward flow in the open field line region, resulting in a lobe cell in the northern ionosphere as originally proposed by Russell [1972]. Type C– reconnection does not affect the ionospheric potentials in the Southern Hemisphere for the pure IMF B_Y case we are considering. (Of course, the corresponding type F+

reconnection on the dawnside does affect the Southern Hemisphere potentials.)

[35] The ionospheric convection driven by type E+ reconnection differs between the two hemispheres. It is this type of reconnection that causes interhemispheric potential mismatch of merging cells. We first consider the Northern Hemisphere. The X line of type E+ reconnection is mapped to a line outside the northern polar cap (E_4 in Figure 9a) owing to the B_N effect on the ε_2 surface (Figure 8c). Consequently, type E+ reconnection drives a sunward flow in the closed field line region. As Figure 9a indicates, the sunward flow is part of the round merging cell, and along the streamlines, type E+ reconnection is first followed by type A+ reconnection and then by type G+ reconnection. This means that type E+ reconnection and type A+ and type G+ reconnection are coupled as we discuss in section 5.2.

[36] The process of type E+ reconnection that drives a sunward flow in the closed field line region is topologically the same as the internal reconnection between overdressed lobe field lines and closed flankside field lines described by Tanaka [1999] and Watanabe *et al.* [2004, 2005, 2006]. For the case of pure northward IMF and significant dipole tilt [Watanabe *et al.*, 2005, 2006], the sunward flow is part of a “reciprocal cell” that circulates exclusively in the closed field line region. In contrast, for the case of oblique northward IMF (at 45° clock angle) and no dipole tilt [Tanaka, 1999; Watanabe *et al.*, 2004], the sunward flow is part of a round merging cell, and the magnetic flux is returned to the nightside via the open field line region. The situation for the type E+ reconnection for pure IMF B_Y is the same as the latter case.

[37] We next consider E+ reconnection effects in the Southern Hemisphere. The X line of type E+ reconnection is mapped to two segments of the polar cap boundary in the southern ionosphere as shown by E_1 and E_3 in Figure 9b. For simplicity, we have assumed that the projected X lines of type E+ reconnection (E_1 and E_3) are sandwiched between the projected X lines of type A and type G reconnection (A_3 and G_1). This configuration is the most probable case for pure IMF B_Y conditions. (Other possible configurations will be discussed in the last paragraph of this section.) Thus type E+ reconnection drives an open-to-closed flow across the dayside polar cap boundary and a closed-to-open flow across the nightside polar cap boundary. These flow directions are the opposite of those driven by type A+ and type G+ reconnection. The net potential drop along segment A_3 - E_1 (segment E_3 - G_1) is $\phi_{A+} - \phi_{E+}$ ($\phi_{G+} - \phi_{E+}$), where $\phi_{A+} = \phi_{G+} > \phi_{E+}$ in the steady state. Consequently, there is a potential difference of ϕ_{E+} between the merging cells in the two hemispheres.

[38] In Figure 9b, one may think that the E_1 - E_3 pair forms a counterclockwise merging cell 2-7-6-3-2 in the Southern Hemisphere. However, this is not a correct interpretation for the present case, because there is no actual magnetic flux transport from 7 to 6 and from 3 to 2. Rather we should interpret Figure 9b as meaning that E_1 (E_3) is paired with A_3 (G_1) and the E_1 - A_3 (E_3 - G_1) pair forms a clockwise merging cell 1-2-7-8-1 (3-4-5-6-3). This will be discussed in section 5.2.

[39] Topologically, there are other possibilities in the X line projection to the southern ionosphere. The segment E_1 in Figure 9b can either be overlapped with A_3

or be at earlier local time than A_3 . This switch in position is possible because E_1 (A_3) is located poleward (equatorward) of the polar cap boundary. Similarly, E_3 in Figure 9b can either be overlapped with G_1 or be at later local time than G_1 , because E_3 (G_1) is located equatorward (poleward) of the polar cap boundary. When E_1 is overlapped with A_3 or when E_3 is overlapped with G_1 , the resultant convection pattern is basically the same as Figure 9b, and the merging cell potential in the Southern Hemisphere becomes lower than the Northern Hemisphere by ϕ_{E+} . In the other cases the resultant convection patterns exhibit dual merging cells. One of such cases is actually observed. When the X line projection is in the order E_1 - A_3 - E_3 - G_1 with increasing local time and the E_1 - A_3 (E_3 - G_1) pair is located in the prenoon (premidnight) region, the resultant convection pattern is the “exchange cell” configuration for oblique northward IMF (45° clock angle) described by Watanabe *et al.* [2004, Figure 3b]. This indicates that although the apparent convection pattern is somewhat different, underlying topology is basically the same for pure IMF B_Y and for oblique northward IMF.

5.2. Magnetic Flux Circulation in the Magnetosphere

[40] We now return to Figure 7 and consider how magnetic flux circulates in the magnetosphere. We first consider magnetic flux circulation associated with the lobe cell. Type C– reconnection converts “relaxed” lobe field flux on the nightside (labeled 9 in Figure 7b) to overdressed lobe field flux on the dayside (labeled 10 in Figure 7b). (Here “relaxed” is used as an antonym of overdressed.) The new overdressed field line 10 in the right panel of Figure 7b is directly transported to the magnetotail by frozen-in convection and becomes field line 9 in the left panel of Figure 7b, participating there in type C– reconnection again. This is the magnetospheric counterpart of the lobe cell in Figure 9a.

[41] We next consider the magnetic flux circulation associated with the merging cells. As noted in section 5.1, type E+ reconnection and type A+ and type G+ reconnection are partly coupled. Type A+ reconnection produces two open field lines (1 and 1' in Figure 7a). The North Lobe field line 1' is transported directly to the magnetotail by frozen-in convection and becomes field line 4' in Figure 7d (see also Figure 9a). Meanwhile, while some of the newly created South Lobe field lines are transported directly to the magnetotail (field line 1 in Figure 7a becomes field line 4 in Figure 7d; see also Figure 9b), the others drape over the dayside magnetosphere (field line 1 in Figure 7a becomes field line 2 in Figure 7c). In Figure 9b the footpoint of the latter overdressed field line moves from 1 to 2. When the field line reaches point 2, it undergoes a “magnetic flux exchange” by type E+ reconnection. Type E+ reconnection converts dayside overdressed open magnetic flux (labeled 2) to nightside “relaxed” open magnetic flux (labeled 3). At the same time, it converts nightside closed magnetic flux (labeled 6) to dayside closed magnetic flux (labeled 7). In the southern ionosphere, the open field line footpoint moves tailward from 2 to 3 in Figure 9b, while the closed field line footpoint moves sunward from 6 to 7 in Figure 9b. Thus there is an apparent tailward open magnetic flux transport and an apparent sunward closed magnetic flux transport in association with type E+ reconnection. This magnetic flux ex-

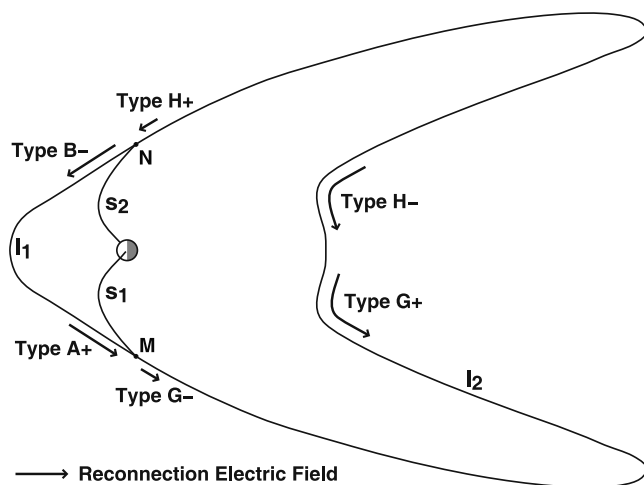


Figure 10. A top view of the separators with reconnection electric fields.

change plays an essential role in the magnetic flux circulation that involves overdamped field lines, as discussed by *Watanabe et al.* [2004, 2005, 2006]. After type E+ reconnection, the new open field line 3 in Figure 7c is now transported directly to the magnetotail and becomes field line 4 in Figure 7d (the footpoint moves from 3 to 4 in Figure 9b). Subsequently, in Figure 7d, field line 4 reconnects with field line 4' in the magnetotail, and a new closed field line (labeled 5) is created. The new closed field line 5 in Figure 7d relaxes after type G+ reconnection and becomes field line 6 in Figure 7c (the footpoints move from 5 to 6 in Figures 9a and 9b), and it then participates in type E+ reconnection again. After type E+ reconnection, the new closed field line 7 in Figure 7c becomes field line 8 in Figure 7a (the footpoints move from 7 to 8 in Figures 9a and 9b), and it then participates in type A+ reconnection again. Thus magnetic flux is returned to the initial state, and one magnetic flux circulation cycle is completed.

[42] Note that the above-described magnetic flux circulation for pure IMF B_Y (90° clock angle) is essentially the same as that for oblique northward IMF (45° clock angle) discussed in terms of “exchange cells” by *Watanabe et al.* [2004]. The only difference is whether the overdamped field lines produced by type A+ reconnection (field line 1 in Figure 7a) move duskward (for 90° clock angle, which is the case considered in this paper) or dawnward (for 45° clock angle) after the reconnection. For the latter case the field line marked “SB” in Figure 1 of *Watanabe et al.* [2004] corresponds to field line 1 in Figure 7a.

6. Deviations of the MHD Simulation Results From the Conceptual Merging Model

6.1. Antisunward Shift of the Round Merging Cell Potential Peak on the Polar Cap Boundary From the Stemline Footpoint

[43] In the conceptual merging model described in Figures 7–9, the potential peak on the polar cap boundary associated with a round merging cell is the stemline footpoint (Figure 9a). In the MHD simulation results (Figure 1), the potential peak (the duskside arrow) is located somewhat

antisunward of the stemline footpoint (point m). The potential difference between the two points is 4.1 kV. This discrepancy may arise from the physical limitation of the numerical model employed in the magnetosphere-ionosphere coupling procedure. However, we also suggest that the discrepancy may reflect another reconnection process not involved in the model described in Figures 7–9. The potential peak shifts antisunward if type G– reconnection occurs. Although type G– reconnection is the reversal process of the normal reconnection on the nightside, it is possible under the geometry of the simulated magnetosphere. Figure 10 shows a top view of the separators encircling the Earth, with arrows indicating reconnection electric fields on the separators. As noted previously, the torus has a wing structure on the flanks, and separator l_2 runs duskward from null M before turning downward. This portion of separator l_2 still lies on the magnetopause, and closed field lines can contact incoming IMF lines at separator l_2 . Thus Closed- α and IMF- γ field lines can merge along separator l_2 (type G– reconnection).

6.2. Equatorward Shift of the Crescent Cell Center From the Polar Cap Boundary

[44] In the merging model described in Figures 7–9, the potential maximum/minimum of the crescent cell (i.e., the center of the cell) is on the polar cap boundary. In the MHD simulation results (Figure 1), the center of the dawnside crescent cell is located equatorward of the polar cap boundary. The potential difference between the crescent cell center and the potential peak on the polar cap boundary (the dawnside arrow) is 4.3 kV. This potential difference may be interpreted as the potential drop of a “viscous” cell. Here, by enclosing in double quotes, we take a neutral position on its origin. A similar equatorward shift of the crescent cell potential peak is seen in the MHD simulation results of *Siscoe et al.* [2001b, Figure 4]. In contrast, in the MHD simulation results by *Crooker et al.* [1998, Figure 3], the potential peak of the dawnside crescent cell is located roughly on the polar cap boundary; the same feature was obtained by K. Kabin et al. (personal communication, 2006, one of the simulation results of *Kabin et al.* [2004]) using an old version of the BATS-R-US code. Thus, although we cannot assess the exact cause of the difference, whether the potential peak shift is significant or not depends on the simulation code (presumably on how the magnetosphere-ionosphere coupling is modeled). Observationally, both cases (crescent cells with and without a “viscous” cell) exist [*Lu et al.*, 1994, Plates 1–4], but it seems more often the case that the potential peak is located equatorward of the polar cap boundary, as seen in examples shown by *Eriksson et al.* [2002, Figures 3–5; 2003, Figures 2 and 5]. What is clear at the moment is that this equatorward shift of the crescent cell potential peak remains unexplained with the conceptual merging model presented in this paper.

7. Conclusions

[45] When the IMF B_Y component is dominant, ionospheric convection exhibits a basic two-cell pattern but with significant dawn-dusk and interhemispheric asymmetries. For IMF $B_Y > 0$, for example, the duskside merging cell potential in the Northern Hemisphere is much higher than

that in the Southern Hemisphere, and the dawnside merging cell potential in the Southern Hemisphere is much higher than that in the Northern Hemisphere. We propose that this interhemispheric potential mismatch originates from reconnection of overdraped lobe field lines and closed flankside field lines (type E+ reconnection in the northern dusk quadrant and type D- reconnection in the southern dawn quadrant for IMF $B_Y > 0$; type E- reconnection in the northern dawn quadrant and type D+ reconnection in the southern dusk quadrant for $B_Y < 0$). This type of north-south asymmetric reconnection does not affect the merging cell potentials in the same hemisphere as the reconnection point (see Figure 9a), whereas in the opposite hemisphere (see Figure 9b), it diminishes the potential of the duskside (or dawnside) Dungey-type merging cell. Thus the total duskside (or dawnside) merging cell potential in one hemisphere is smaller than that in the other hemisphere by the corresponding reconnection voltage (ϕ_{E+} , ϕ_{D-} , ϕ_{E-} , or ϕ_{D+}).

[46] **Acknowledgments.** M. Watanabe was funded by a Natural Sciences and Engineering Research Council (NSERC) Canada Collaborative Research Opportunities (CRO) grant for "Scientific Personnel for the Canadian SuperDARN Program" (G. Sofko, PI) and by a Canadian Space Agency (CSA) Space Science Enhancement Program (SSEP) grant. K. Kabin and R. Rankin were supported by the CSA and NSERC; they also acknowledge the use of WestGrid computational resources. A. Ridley was supported by NASA Geospace grant NNG04GK18G. R. Clauer was supported by NSF ITR grant ATM-0325332. T. Gombosi was supported by NASA AISRP grant NNG04GP89G.

[47] Wolfgang Baumjohann thanks the reviewers for their assistance in evaluating this paper.

References

- Alekseyev, I. I., and Y. S. Belen'kaya (1983), Electric field in an open model of the magnetosphere, *Geomagn. Aeron.*, **23**, 57–61.
- Burch, J. L., P. H. Reiff, J. D. Menietti, R. A. Heelis, W. B. Hanson, S. D. Shawhan, E. G. Shelley, M. Sugiura, D. R. Weimer, and J. D. Winningham (1985), IMF B_Y -dependent plasma flow and Birkeland currents in the dayside magnetosphere: 1. Dynamics Explorer observations, *J. Geophys. Res.*, **90**(A2), 1577–1593.
- Cowley, S. W. H. (1973), A qualitative study of the reconnection between the Earth's magnetic field and an interplanetary field of arbitrary orientation, *Radio Sci.*, **8**, 903–913.
- Crooker, N. U. (1990), Morphology of magnetic merging at the magnetopause, *J. Atmos. Terr. Phys.*, **52**, 1123–1134.
- Crooker, N. U. (1992), Reverse convection, *J. Geophys. Res.*, **97**(A12), 19,363–19,372.
- Crooker, N. U., G. L. Siscoe, and F. R. Toffoletto (1990), A tangent sub-olar merging line, *J. Geophys. Res.*, **95**(A4), 3787–3793.
- Crooker, N. U., J. G. Lyon, and J. A. Fedder (1998), MHD model merging with IMF B_Y : Lobe cells, sunward polar cap convection, and overdraped lobes, *J. Geophys. Res.*, **103**(A5), 9143–9151.
- Dungey, J. W. (1961), Interplanetary magnetic field and the auroral zones, *Phys. Rev. Lett.*, **6**, 47–48.
- Dungey, J. W. (1963), The structure of the exosphere or adventures in velocity space, in *Geophysics: The Earth's Environment*, edited by C. DeWitt, J. Hieblot, and A. LeBeau, pp. 503–550, Gordon and Breach, New York.
- Eriksson, S., J. W. Bonnell, L. G. Blomberg, R. E. Ergun, G. T. Marklund, and C. W. Carlson (2002), Lobe cell convection and field-aligned currents poleward of the region 1 current system, *J. Geophys. Res.*, **107**(A8), 1185, doi:10.1029/2001JA005041.
- Eriksson, S., W. J. Peria, J. W. Bonnell, Y.-J. Su, R. E. Ergun, Y.-K. Tung, G. K. Parks, and C. W. Carlson (2003), Lobe cell convection and polar cap precipitation, *J. Geophys. Res.*, **108**(A5), 1198, doi:10.1029/2002JA009725.
- Fukao, S., M. Ugai, and T. Tsuda (1975), Topological study of magnetic field near a neutral point, *Rep. Ionos. Space Res. Jpn.*, **29**, 133–139.
- Greene, J. M. (1988), Geometrical properties of three-dimensional reconnecting magnetic fields with nulls, *J. Geophys. Res.*, **93**(A8), 8583–8590.
- Hesse, M., J. Birn, and K. Schindler (1990), On the topology of flux transfer events, *J. Geophys. Res.*, **95**(A5), 6549–6560.
- Kabin, K., R. Rankin, G. Rostoker, R. Marchand, I. J. Rae, A. J. Ridley, T. I. Gombosi, C. R. Clauer, and D. L. DeZeeuw (2004), Open-closed field line boundary position: A parametric study using an MHD model, *J. Geophys. Res.*, **109**, A05222, doi:10.1029/2003JA010168.
- Lau, Y.-T., and J. M. Finn (1990), Three-dimensional kinematic reconnection in the presence of field nulls and closed field lines, *Astrophys. J.*, **350**, 672–691.
- Lu, G., et al. (1994), Interhemispheric asymmetry of the high-latitude ionospheric convection pattern, *J. Geophys. Res.*, **99**(A4), 6491–6510.
- Powell, K. G., P. L. Roe, T. J. Linde, T. I. Gombosi, and D. L. DeZeeuw (1999), A solution-adaptive upwind scheme for ideal magnetohydrodynamics, *J. Comput. Phys.*, **154**, 284–309.
- Reiff, P. H., and J. L. Burch (1985), The IMF B_Y -dependent plasma flow and Birkeland currents in the dayside magnetosphere: 2. A global model for northward and southward IMF, *J. Geophys. Res.*, **90**(A2), 1595–1609.
- Ridley, A. J., T. I. Gombosi, and D. L. DeZeeuw (2004), Ionospheric control of the magnetosphere: Conductance, *Ann. Geophys.*, **22**, 567–584.
- Russell, C. T. (1972), The configuration of the magnetosphere, in *Critical Problems of Magnetospheric Physics*, edited by E. R. Dyer, pp. 1–16, Inter-Union Comm. on Sol. Terr. Phys. Sec., Natl. Acad. of Sci., Washington, D. C.
- Schindler, K., M. Hesse, and J. Birn (1988), General magnetic reconnection, parallel electric fields, and helicity, *J. Geophys. Res.*, **93**(A6), 5547–5557.
- Siscoe, G. L. (1988), The magnetospheric boundary, in *Physics of Space Plasmas (1987)*, edited by T. Chang, G. B. Crew, and J. R. Jasperse, pp. 3–78, Sci. Publ., Cambridge, Mass.
- Siscoe, G. L., G. M. Erickson, B. U. Ö. Sonnerup, N. C. Maynard, K. D. Siebert, D. R. Weimer, and W. W. White (2001a), Magnetospheric sash dependence on IMF direction, *Geophys. Res. Lett.*, **28**(10), 1921–1924.
- Siscoe, G. L., G. M. Erickson, B. U. Ö. Sonnerup, N. C. Maynard, K. D. Siebert, D. R. Weimer, and W. W. White (2001b), Global role of E_{\parallel} in magnetopause reconnection: An explicit demonstration, *J. Geophys. Res.*, **106**(A7), 13,015–13,022.
- Song, P., D. L. DeZeeuw, T. I. Gombosi, J. U. Kozyra, and K. G. Powell (2001), Global MHD simulations for southward IMF: A pair of wings in the flanks, *Adv. Space Res.*, **28**(12), 1763–1771.
- Sonnerup, B. U. Ö. (1988), On the theory of steady state reconnection, *Comput. Phys. Commun.*, **49**, 143–159.
- Tanaka, T. (1999), Configuration of the magnetosphere-ionosphere convection system under northward IMF conditions with nonzero IMF B_Y , *J. Geophys. Res.*, **104**(A7), 14,683–14,690.
- Vasyliunas, V. M. (1975), Theoretical models of magnetic field line merging, 1, *Rev. Geophys.*, **13**, 303–336.
- Vasyliunas, V. M. (1984), Steady state aspects of magnetic field line merging, in *Magnetic Reconnection in Space and Laboratory Plasmas*, *Geophys. Monogr. Ser.*, vol. 30, edited by E. W. Hones Jr., pp. 25–31, AGU, Washington, D. C.
- Watanabe, M., G. J. Sofko, D. A. André, T. Tanaka, and M. R. Hairston (2004), Polar cap bifurcation during steady-state northward interplanetary magnetic field with $|B_Y| \sim B_Z$, *J. Geophys. Res.*, **109**, A01215, doi:10.1029/2003JA009944.
- Watanabe, M., K. Kabin, G. J. Sofko, R. Rankin, T. I. Gombosi, A. J. Ridley, and C. R. Clauer (2005), Internal reconnection for northward interplanetary magnetic field, *J. Geophys. Res.*, **110**, A06210, doi:10.1029/2004JA010832.
- Watanabe, M., G. J. Sofko, D. A. André, J. M. Ruohoniemi, M. R. Hairston, and K. Kabin (2006), Ionospheric signatures of internal reconnection for northward interplanetary magnetic field: Observation of "reciprocal cells" and magnetosheath ion precipitation, *J. Geophys. Res.*, **111**, A06201, doi:10.1029/2005JA011446.
- White, W. W., G. L. Siscoe, G. M. Erickson, Z. Kaymaz, N. C. Maynard, K. D. Siebert, B. U. Ö. Sonnerup, and D. R. Weimer (1998), The magnetospheric sash and the cross-tail S, *Geophys. Res. Lett.*, **25**(10), 1605–1608.
- C. R. Clauer, Department of Electrical and Computer Engineering, Virginia Polytechnic Institute and State University, Blacksburg, VA 24061, USA.
- T. I. Gombosi and A. J. Ridley, Department of Atmospheric, Oceanic, and Space Sciences, University of Michigan, Ann Arbor, MI 48109-2143, USA.
- K. Kabin and R. Rankin, Department of Physics, University of Alberta, Edmonton, AB, Canada T6G 2J1.
- G. J. Sofko and M. Watanabe, Department of Physics and Engineering Physics, University of Saskatchewan, 116 Science Place, Saskatoon, SK, Canada S7N 5E2. (masakazu.watanabe@usask.ca)